Biophysical Journal
Article

Biophysical Society

Modulating Vesicle Adhesion by Electric Fields

Jan Steinkühler,[1] Jaime Agudo-Canalejo,[1] Reinhard Lipowsky,[1] and Rumiana Dimova[1,*]
[1]Max Planck Institute of Colloids and Interfaces, Science Park Golm, Potsdam, Germany

ABSTRACT We introduce an experimental setup for modulating adhesion of giant unilamellar vesicles to a planar substrate. Adhesion is induced by the application of an external potential to a transparent indium tin oxide-coated electrode (the substrate), which enables single-vesicle studies. We demonstrate tunable and reversible adhesion of negatively charged vesicles. The adhesion energy at different potentials is calculated from the vesicle shape assessed with confocal microscopy. Two approaches for these estimates are employed: one based on the whole contour of the vesicle and a second based on the contact curvature of the membrane in the vicinity of the substrate. Both approaches agree well with each other and show that the adhering vesicles are in the weak adhesion regime for the range of explored external potentials. Using fluorescence quenching assays, we detect that, in the adhering membrane segment, only the outer bilayer leaflet of the vesicle is depleted of negatively charged fluorescent lipids, while the inner leaflet remains unaffected. We show that depletion of negatively charged lipids is consistent Poisson-Boltzmann theory, taking into account charge regulation from lipid mobility. Finally, we also show that lipid diffusion is not significantly affected in the adhering membrane segment. We believe that the approaches introduced here for modulating and assessing vesicle adhesion have many potential applications in the field of single-vesicle studies and research on membrane adhesion.

INTRODUCTION

Giant unilamellar vesicles (GUVs) have emerged as a versatile model membrane system (1–4). Applications reach from models of biological membranes to microreactors. In this work, we employ them to study adhesion. In biological systems, adhesion is usually ensured by specific adhesion molecules. However, unspecific forces are always at play. Here, we exploit these interactions and study the adhesion of GUVs to a solid support where adhesion is driven by an external electrical potential.

Adhesion of GUVs has been previously explored both in theoretical and experimental studies (5–11). During adhesion, the vesicle undergoes a shape transformation and repulsive membrane undulations against the rigid surface are suppressed. This energetic cost is balanced by the (attractive) interaction between the surface and the vesicle. Generally, an attractive force can be provided either by specific ligand-receptor bonds or by generic nonspecific interactions arising from van der Waals or electrostatic forces. Some examples of the latter are provided in the following. Bernard et al. (12) have used polylysine-coated surfaces to induce adhesion of electrically neutral GUVs. In another work, reflection interference contrast microscopy was used to study adhesion of GUVs to a positively charged surface coated with 3-amino-propyl-triethoxy-silane (7). In a more recent study, the nonspecific interaction between a pinned lipid membrane patch from a GUV and a substrate coated with the relatively inert protein bovine serum albumin was studied and the resulting interaction potential strength was extracted from the analysis of membrane shape and fluctuations (13). Other studies explored the adhesion of positively charged GUVs to a planar-supported lipid bilayer where the interaction was influenced by changes in bulk pH and hence by modulating the surface charge of the membranes (14,15). In all of these studies, adhesion either was governed by a fixed attractive potential, was irreversible, or had no possibility to directly modulate adhesion of the same vesicle. Formation and desorption of supported lipid bilayers (SLBs) and liposome layers on polarizable electrodes was described in Kumar et al. (16) and GUVs interacting with electrodes were used previously to measure membrane fluctuations (17).

Here, we introduce an experimental approach to induce reversible adhesion of GUVs by means of an externally applied electric potential. The advantage of the approach is that the adhesion strength can be varied easily and gradually for the same vesicle. This method enables single-vesicle studies as the GUV can be observed before

Submitted March 10, 2016, and accepted for publication August 22, 2016.
*Correspondence: rumiana.dimova@mpikg.mpg.de
Editor: Stephen Evans.
http://dx.doi.org/10.1016/j.bpj.2016.08.029

and after adhesion. The process resembles what is known as electrowetting of (aqueous) droplets on a solid support (18,19). We compare two different methods to calculate the adhesion energy from the vesicle morphology observed by confocal microscopy, investigate the partitioning of a fluorescent lipid analog between the unbound vesicle cap and the bound membrane segment, and measure the lipid diffusivity.

MATERIALS AND METHODS

Vesicle preparation and imaging

Vesicles were prepared by electroformation (20). Chloroform stock solutions of 1,2-dioleoyl-*sn*-glycero-3-phosphocholine (DOPC) and 1,2-dioleoyl-*sn*-glycero-3-phospho-(1′-*rac*-glycerol) (sodium salt) (DOPG) were mixed at molar ratio 80:20 with a final lipid concentration of 4 mM. The lipids were obtained from Avanti Polar Lipids (Alabaster, AL). At neutral pH, DOPG contributes a negative surface charge to the formed vesicles. If not indicated differently, the fluorescent analog DiIC18, i.e., 2-[3-(1,3-dihydro-3,3-dimethyl-1-octadecyl-2H-indol-2-ylidene)-1-propenyl]-3,3-dimethyl-1-octadecyl; perchlorate (Molecular Probes, Eugene, OR) was added to the lipid mixture at a concentration of 0.1 mol %. For the dye distribution measurements, 1 mol % of the fluorescent dye 1-oleoyl-2-[12-[(7-nitro-2-1,3-benzoxadiazol-4-yl)amino]dodecanoyl]-*sn*-glycero-3–[phospho-rac-(1-glycerol)] (NBD-PG) ammonium salt (Avanti Polar Lipids) was added. In some experiments, 1-oleoyl-2-[12-[(7-nitro-2-1,3-benzoxadiazol-4-yl)amino]dodecanoyl]-*sn*-glycero-3-phosphocholine (NBD-PC), was added instead. In total, 10 μL of the stock solution were spread on two conductive glasses coated with indium tin oxide (ITO). To eliminate trace amounts of chloroform, the glasses were kept between 2 and 2.5 h under vacuum at room temperature. They were then assembled to form a chamber of 2 mL volume that was filled with sucrose solution (17 mg/mL) buffered with 2 mM HEPES pH 7.4, containing 1 mM EDTA and with a final osmolality of 63 mOsmol/L. All chemicals were obtained from Sigma-Aldrich (St. Louis, MO). Electroformation was carried out at 10 Hz sinusoidal voltage of 630 mV root-mean squared for 2 h and at 300 mV and 5 Hz for an additional 30 min. The vesicles were harvested from the chamber and left to equilibrate overnight at room temperature. Part of the vesicle suspension was mixed with an isoosmolar buffered glucose solution at volume ratio of 1:2 (to a final volume of 90 μL). To provide excess area for adhesion, the vesicles were deflated before imaging by water evaporation from this vesicle suspension at room temperature for 40 min. The steady increase in osmolarity (to a value of ~88 mOsmol/L as measured by the decrease in mass during evaporation) deflated the vesicles in a smooth manner. The density difference between the outside and inside solutions led to sedimentation of the vesicles to the bottom of the chamber. When required, the solution conductivity was measured with SevenEasy (Mettler-Toledo, Greifensee, Switzerland).

Imaging was performed on a confocal SP5 setup (Leica, Mannheim, Germany). DiIC18 was excited with a 581-nm laser line (diode-pumped solid-state laser) and NBD-PG was excited using a 488-nm line (Argon laser). The fluorescence signal was collected between 565 and 670 nm and 494 and 642 nm, respectively. In some experiments, the reflection from the surface of ITO cover glass facing the solution was visualized by scanning with the 488-nm laser line in reflection mode and detecting the reflected light in the range 485–490 nm. Side views or vertical cross sections in the *xz* plane were obtained by moving the specimen along the *z* axis of the microscope by a galvanometer stage (Leica). The image reconstruction was done from consecutive scanning of a *xy* line passing through the axes of symmetry of the vesicle. This enables us to obtain a complete side view with minimal photobleaching. Because the difference between the refractive indices of the objective immersion medium (water) and the sugar solution in the vesicle suspension is far below 1%, spherical aberrations are negligible (see, e.g., Bezlyepkina et al. (21)) and were not considered for correcting the vesicle images in the *z* scans.

Fluctuation analysis

We measured the bending rigidity of the DOPC/DOPG vesicles by fluctuation analysis of the thermally induced motion of the membrane. Details of the method are published in Gracià et al. (22). Experiments were performed on an Axiovert 135 microscope (Zeiss) using a 40× objective in phase contrast mode. Imaging was done with a fast digital camera HG-100K (Redlake, San Diego, CA) using a mercury lamp HBO W/2 as a light source. We acquired 3600 snapshots of each vesicle with an exposure time of 200 μs. Only vesicles with clearly visible fluctuations and no visible defects were considered for the analysis. No difference in the bending rigidity was found for vesicles in sucrose buffer or diluted in glucose buffer within the experimental uncertainty.

Zeta potential measurements

We have measured the zeta potential of large unilamellar vesicles at 0.4 mM DOPC/DOPG 80:20 in the same glucose buffer as used in the GUV experiments. The vesicles were prepared by extrusion through a polycarbonate membrane with a 200-nm pore size using a pneumatic extruder (Avestin, Ottawa, Canada). After 20 extrusion cycles, monodisperse vesicles with an average diameter of 147 nm were obtained as assessed with dynamic light scattering. Dynamic light scattering and electrophoretic mobility were measured using a Zetasizer Nano ZS (Malvern Instruments, Worcestershire, UK). Zeta potentials were deduced from the electrokinetic mobility data using the Smoluchowski approximation. Finally we extracted the surface potential by assuming the ζ-potential shear plane to be 0.2 nm away from the real membrane surface (23).

Setup of the adhesion chamber

The adhesion chamber consisted of two ITO-coated cover glasses with a thickness of 0.17 mm (ITO film thickness $<$ 100 nm; Präzisions Glas & Optik, Iserlohn, Germany), which were separated by a rubber spacer of 1 mm thickness. The vesicle suspension was not in contact with the spacer and was surrounded by air as shown in Fig. S1 in the Supporting Material. The chamber was sealed to prevent evaporation during the experiment. Because the ITO film is transparent, vesicles could be observed with a conventional inverted (confocal) microscope setup. The ITO glasses were connected with conductive copper tapes to an external signal generator (Model 33220A; Agilent Technologies Deutschland, Böblingen, Germany) and direct current (DC) voltage was applied with the bottom glass connected to the positive terminal. In series with the voltage source, the electric current was measured using a digital multimeter (Model 2000; Keithley Instruments, Cleveland, OH). The whole chamber was closed and held together by two custom-made metal plates and fitted on the stage of the microscope (Fig. S1).

Quenching assay and fluorescence intensity measurements

NBD-PG located in the outer leaflet of the vesicles membrane was quenched by reduction with dithionite (24). We first prepared 1 M stock solution of sodium dithionite (Sigma-Aldrich) in the sucrose buffer used for vesicle preparation. Then, 1 μL of this quenching buffer was pipetted into 100 μL of vesicle suspension in sucrose buffer. The solution was gently stirred to ensure homogenous distribution of the quenching agent. The vesicles were then incubated for 15 min and consecutively diluted in isoosmolar glucose buffer as done with vesicles not treated with quencher. On the

timescales of the observations, no or insignificant leakage of quenching agent into the vesicle interior occurred. The quenching of the external leaflet of the vesicle membrane was confirmed by the decrease of fluorescence to approximately one-half the original value (fluorescence from both leaflets).

Fluorescent intensities of quenched and unquenched vesicles were determined by the peak of a Gaussian fit to the intensity line profile across the membrane perpendicular to the cover glass. The peak value of the Gaussian was then used for further analysis. Examples for fitting an unquenched and a quenched vesicle are shown in Fig. S2. In addition to single vesicle studies, we also obtained statistically relevant results by analyzing at least eight different vesicles from two different batches. Vesicles that exhibited visible defects, pinning to the surface, or did not react to the external voltage because of local surface defects, were not considered for further analysis. For all measurements, the settings of the confocal setup were kept fixed.

Fluorescence recovery after photobleaching measurements

NBD-PG was bleached using the 488-nm line of the confocal microscope. A circular spot with diameter 5 μm in the xy plane both in the adhering membrane segment and at the north pole of a vesicle was bleached for 420 ms. Afterwards, imaging was done at nonbleaching laser intensity for 7 s. The intensity-time trace was then fitted to the commonly used one-component recovery model (25). At least five individual bleaching curves per vesicle were obtained.

Theory for strong adhesion regime

The adhesion energy was obtained from the global shape of the vesicle. In the absence of a spontaneous curvature of the membrane, the equilibrium shape of a vesicle adhering to a planar substrate is determined by the bending rigidity of the membrane, κ, and the adhesion energy per unit area, W, as well as by the total membrane area A and enclosed volume V of the vesicle. This minimum energy shape can, in general, only be calculated numerically (5). If the adhesion is strong, the vesicle tries to maximize its contact area and attains a shape that is very close to a spherical cap (5). The latter shape is characterized by the effective contact angle θ_0 (see Fig. 1 A), which is solely determined by the reduced volume $V/A^{3/2}$ according to

$$\frac{8-9\cos\theta_0+\cos 3\theta_0}{12\sqrt{\pi}(2-2\cos\theta_0+\sin^2\theta_0)^{3/2}}=\frac{V}{A^{3/2}}. \qquad (1)$$

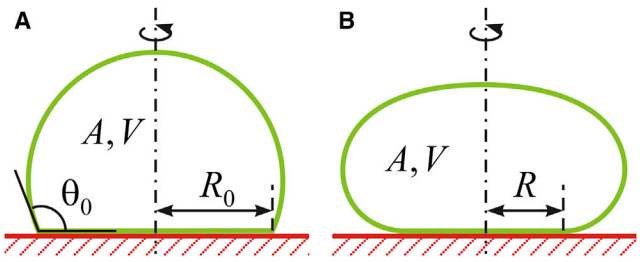

FIGURE 1 Sketches of the same vesicle with total area A and enclosed volume V (A) in the strong adhesion limit and (B) for smoothly curved membrane close to the contact line. In (A), the shape is that of a spherical cap and the values of the effective contact angle θ_0 and the radius of the adhering membrane segment R_0 are fixed by A and V through Eq. 1. In (B), the shape deviates from a spherical cap and the radius of the adhering membrane segment $R<R_0$ is given by Eq. 4.

In the strong adhesion limit, the circular contact area of the spherical cap has the radius

$$R_0=\sqrt{\frac{A[1+\cos(\theta_0)]}{\pi[3+\cos(\theta_0)]}}. \qquad (2)$$

In the limit of small contact angles, one obtains a pancake with contact area $\pi R_0^2=A/2$ and vanishing volume V.

When the contact region close to the contact line is viewed with sufficiently high resolution, the contour of the vesicle membrane does not exhibit a sharp contact angle, which would imply an infinite bending energy, but rather a smoothly curved membrane segment with contact curvature radius

$$R_{\mathrm{co}}=\sqrt{\frac{\kappa}{2W}}. \qquad (3)$$

Thus, deviations of the vesicle shape from the spherical cap shape can be expanded in powers of $R_{\mathrm{co}}/\sqrt{A}$, where $\sqrt{A}$ describes the linear size of the vesicle membrane. Such an expansion was first performed for an adhering pancake with $\theta_0=0$ (26) and later generalized to arbitrary values of θ_0 (27). In the general case, one finds that the actual radius R of the contact area is given by (27)

$$R=R_0-\sqrt{\frac{2\kappa}{W}}\,\frac{\cos(\theta_0/2)}{1+\sin(\theta_0/2)}+O\left(\frac{\kappa}{W\sqrt{A}}\right). \qquad (4)$$

If we solve this equation for W/κ, we obtain

$$\frac{W}{\kappa}\approx\frac{2}{(R-R_0)^2}\left(\frac{\cos(\theta_0/2)}{1+\sin(\theta_0/2)}\right)^2, \qquad (5)$$

to leading order in $R-R_0$.

First method of image analysis: adhesion energy from overall vesicle shape

For each vesicle, we acquire a series of confocal images for increasing values of the applied voltage (Fig. 2). Each confocal image contains a vertical cross section of the vesicle. The vesicle contour is then identified manually, as shown in Fig. S3. Assuming that the shapes are axisymmetric (which is confirmed from three-dimensional projection images of the adhering vesicle), we can obtain the total membrane area A and enclosed volume V of the vesicle by integration along the contour for each value of the applied voltage. Both the area and the volume of the vesicles are found to remain constant within experimental error as the voltage is increased. Note that the assessment of the adhesion energy does not require that the volume nor the area remain constant. In addition, the radius R of the adhering membrane segment can be directly measured and is found to increase with increasing applied voltage. By inserting the measured values of A and V into Eq. 1 and solving it numerically, we obtain the values of the effective contact angle θ_0 and the radius R_0 of the adhering membrane segment corresponding to the spherical cap limit. These calculated values, together with the measured value of the radius R of the adhering membrane segment, can then be inserted in Eq. 5 to obtain the reduced adhesion energy per unit area, W/κ. This procedure was repeated for each vesicle at each value of the applied voltage. The corresponding error $\Delta(W/\kappa)$ is determined by linear propagation of the experimental uncertainties ΔA, ΔV, and ΔR in Eq. 5. Finally, a value for the adhesion energy per unit area, averaged over all vesicles, is computed for each applied voltage by calculating the weighted arithmetic mean of W/κ for different vesicles at a certain voltage, with the weight given by the inverse variance $1/[\Delta(W/\kappa)]^2$.

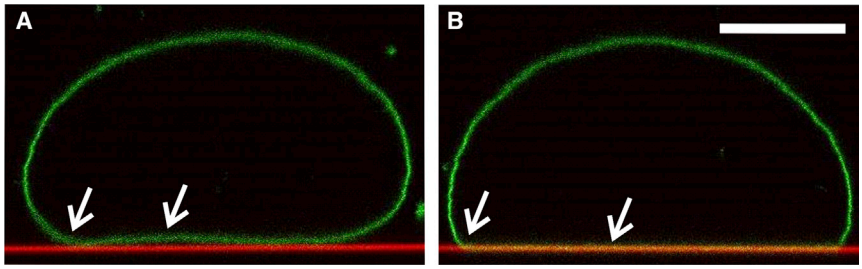

FIGURE 2 Confocal images of the vertical cross sections of a GUV made of DOPC/DOPG 80:20. The scale bar represents 20 μm. The membrane fluorescence is shown in green and the reflection from the ITO surface is shown in red. (*A*) Nonadhering vesicle in the absence of applied voltage. Note the smoothly curved membrane (*left arrow*) as compared to the case of adhesion in (*B*). (*Right arrow*) Undulation of the bound membrane segment, indicating a relatively large separation of this segment from the ITO substrate. (*B*) Same vesicle adhering to the substrate upon application of 1 V DC field. (*Left arrow*) Appearance of an effective contact angle; (*right arrow*) absence of any visible undulation in the vicinity of the surface, which also demonstrates the increased adhesion.

Measuring membrane tension from contour analysis

The membrane tension of the vesicle can be estimated in a similar manner as the adhesion strength, by considering the deviations of the vesicle shape from a spherical cap, which corresponds to the limit of strong adhesion. The combined bending and adhesion free energies of a vesicle with given area A and enclosed volume V can be approximated by (27)

$$F = -W\pi R_0^2 + 8\sqrt{\pi\kappa W A}\,\frac{1-\sin\left(\frac{\theta_0}{2}\right)}{\sqrt{3+\cos\theta_0}} + O(\kappa), \qquad (6)$$

where we use the same notation as in the previous section. In mechanical equilibrium, the tension Σ of the vesicle membrane will then be given by (28) $\Sigma = -\partial F/\partial A\,|_V$, taking into account that both R_0 and θ_0 depend on the vesicle area. One thus finds for the tension

$$\Sigma = \frac{W}{1+\cos\theta_0} - \sqrt{\frac{4\pi\kappa W}{A}}\,\frac{\sqrt{3+\cos\theta_0}\left[2\sin\left(\frac{\theta_0}{2}\right)+\cos\theta_0\right]}{1+\cos\theta_0} + O(\kappa/A). \qquad (7)$$

The first term on the right-hand side of this equation represents the well-known Young relation for liquid droplets; the second term provides a correction arising from the bending rigidity of the membrane. Combining Eqs. 5 and 7 to eliminate the adhesion strength, we can estimate the tension of the membrane by simply measuring its enclosed volume V, total area A, and radius R of the adhering membrane segment via the relation

$$\frac{\Sigma}{\kappa} \approx \frac{1}{(R_0-R)^2\left[\sin\left(\frac{\theta_0}{4}\right)+\cos\left(\frac{\theta_0}{4}\right)\right]^4}, \qquad (8)$$

where R_0 and θ_0 are determined by the measured volume and area via Eq. 1. Note that the membrane tension as given by Eq. 8 is always positive. This implies that the vesicle membrane is stretched with the area increase $A - A_0$ satisfying $\Sigma = K_A((A-A_0)/A_0)$, where K_A is the membrane area compressibility modulus and A_0 is the optimal (relaxed) area of the vesicle.

Second method of image analysis: adhesion energy from contact curvature

We extracted the contact curvature radius R_{co} (see Eq. 3) from 10 adhering vesicles at different adhesion strengths, by fitting the contour in the contact zone with a circle. To find the optimal circle radius we used a refined fitting method, in which we follow the goodness of fit while increasing the part of the membrane segment considered for fitting and select the fit with the best-adjusted coefficient of determination. A typical example is shown in Fig. S4. This optimal radius is assigned to the contact curvature R_{co} and Eq. 3 is used to estimate the adhesion energy independently of the method based on the whole-vesicle contour described above.

Numerical solution and parameter estimation of the charge regulated Poisson-Boltzmann equation

We solve the Poisson-Boltzmann equation for the dimensionless electrostatic potential $\psi = e\varphi/k_BT$ with k_B as the Boltzmann constant, and T as the temperature:

$$\nabla^2\psi = \lambda^{-2}\sinh\psi, \qquad (9)$$

where $\lambda = (\varepsilon_0\varepsilon_r k_B T/2c_0e^2)^{1/2}$ is the Debye length for a solution of monovalent salt of bulk concentration c_0 and dielectric constant ε_r. We did not directly control the ionic strength in the used buffers, which is set by the buffer concentration, adjustment of pH, and impurities in the used reagents. However, from conductivity measurements, we estimated the equivalent ionic strength of 2 mM NaCl solution, which implies Debye length $\lambda \cong 7$ nm. The special boundary condition $-\alpha\nabla\psi\cdot\mathbf{n} = (e^{-(\psi+\psi_0)}/(1-\phi)/\phi + e^{-(\psi+\psi_0)})$ self-consistently accounts for the charge regulation due to lipid exchange with a lipid reservoir. Here, ψ_0 denotes the resting potential of an isolated membrane and was set to –63 mV, as obtained from the ζ-potential measurements; $\mathbf{n}$ is the normal vector to the lipid plane, $\alpha = a\varepsilon_0\varepsilon_r k_B T/e^2$ with $a = 70$ Å as the surface area of a typical lipid; and $\phi = 0.2$ is the fraction of charged lipids in our experiments. This boundary condition was derived earlier in Harries et al. (29) and May et al. (30). The ITO surface was considered as an ideal (current blocking) electrode, where the charges $Q_e = C_{if}(U - U_0)$ are fixed by the applied potential and the capacitance of the ITO-electrolyte interface and is set to $C_{if} = 8\times10^6$ F/cm^2 and $U_0 = 540$ mV (31). The solutions of the Poisson-Boltzmann equation were computed using COMSOL Ver. 3.5a for 10 separation distances between 0.1λ and 4λ on a one-dimensional mesh consisting of 60 elements. The contour plots were generated by spline interpolation between the discrete simulation results.

RESULTS AND DISCUSSION

Adhesion of a deflated GUV is shown in Fig. 2. In the absence of the DC field, the vesicle is free to move (in the case of convection in the chamber) and exhibits visible thermal fluctuations, which are suppressed when the vesicle starts to adhere at a threshold voltage of ~0.8 V. The vesicle undergoes a shape transition from an unbound to a bound

state and the thermal undulations in the lower part of the vesicle in close contact with the ITO surface are suppressed. With further increase of the external voltage, adhesion is smoothly regulated by the applied voltage and the vesicles spread further over the surface, increasing the area of the adhering membrane segment. The effective contact angle decreases with increasing contact area arising from the constraints of fixed membrane area and vesicle volume. Note that GUVs cannot adapt their surface area freely, in contrast to liquid droplets sitting on a surface. Electroformed vesicles are characterized by different initial tensions and degree of deflation in the same batch and we could observe that tenser vesicles do not wet the surface as much as well-deflated vesicles. After the voltage is switched off, the membrane segment in the contact area is again free to fluctuate and the effective contact angle approaches 180°. The shape change induced by adhesion can be completely reversible (Fig. S5). In some cases, however, the original overall vesicle shape is not fully recovered, indicating a change in the vesicle area/volume during adhesion. To probe for changes in the volume, we used phase contrast microscopy to check for leakage of sucrose encapsulated in the vesicles due to formation of pores. No decrease in contrast over the whole range of used voltages was observed (data not shown). Hence, no or only an insignificant amount of leakage occurred due to the adhesion. The vesicle volume as deduced from shape analysis was also found constant. We thus speculate that the change in the area/volume arose from a change in the apparent vesicle area. It is plausible that during adhesion, membrane reservoirs such as tubes or membrane invaginations are pulled out to the vesicle surface. Electroformed GUVs are known to frequently exhibit such hidden membrane reservoirs (2,32).

Calculated adhesion energies at varied external potential

Following the first method of image analysis as described in the Materials and Methods, we determined the adhesion energy from the overall vesicle shape as detected by confocal microscopy images recorded for different external potentials (Fig. 3 *A*). To the best of our knowledge, this is the first time the adhesion energies were directly calculated from vesicle images obtained by confocal microscopy. In agreement with the optical observations, at a threshold voltage of ~0.8 V, a sharp monotonic increase in adhesion energy was measured.

Because the method yields only the reduced adhesion energy W/κ, we have independently measured the bending rigidity κ of nonadhering vesicles by fluctuation analysis (see Materials and Methods). In total, 20 vesicles were analyzed. For the bending rigidity measured at 23°C, we obtained $\kappa \cong 20 \pm 2\ k_BT$. The deduced value for the bending rigidity is significantly lower than that measured

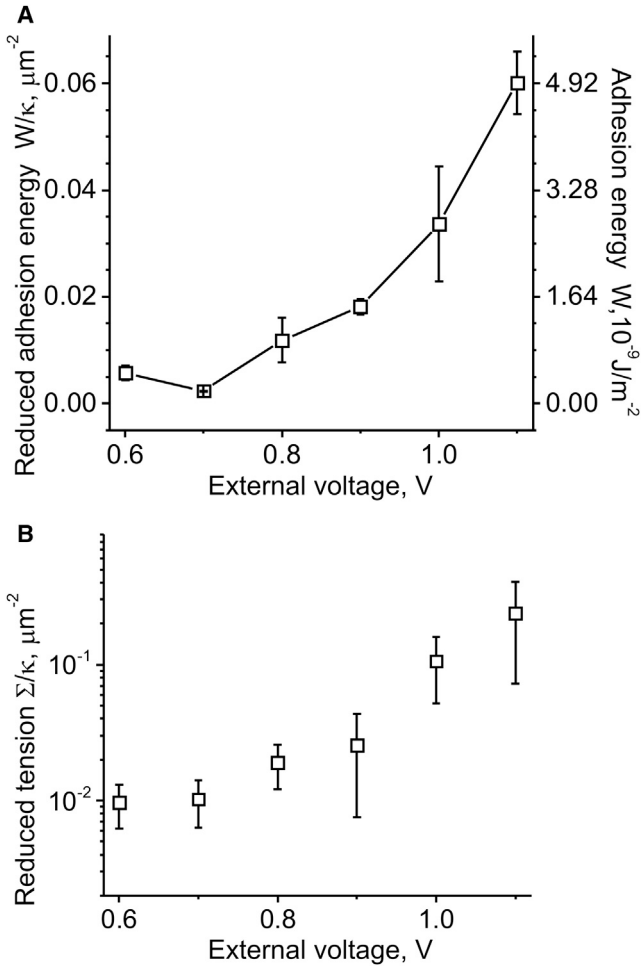

FIGURE 3 Adhesion energy and membrane tension in DOPC/DOPG 80:20 vesicles adhering to an ITO substrate as a function of applied external potential. (*A*) Adhesion energies of overall 24 vesicles at different external potentials. The data are obtained from the analysis of the overall vesicle shape; see Materials and Methods for details. (*Left axis*) Reduced adhesion energy per unit area, W/κ; (*right axis*) absolute value of the adhesion energy per unit area, assuming that the bending rigidity is not influenced by the applied voltage. (*B*) Reduced vesicle tension of a single vesicle at different external potentials, i.e., adhesion energies.

for DOPC/DOPG 90:10 membranes at pH 5 (33), indicating a rather strong dependence of the bending rigidity on the protonation state of the lipids and hence the surface charge of the membrane as well as the used buffers (34). Using the measured value of the bending rigidity and assuming that it is not influenced by the adhesion process, we were able to calculate the absolute value of the adhesion energy in our experiments (see *right axis* in Fig. 3 *A*). The explored adhesion energies are relatively low and belong to the regime of weak adhesion. Note that as we will show later, the lipids may redistribute between the bound and unbound part of the vesicle, which might lead to changes in the bending rigidity of the membrane. Thus, in the following, we will present the results in terms of reduced adhesion energy W/κ.

From the overall vesicle shape, we were also able to extract the induced tension as described in the Materials and Methods. As expected, with increasing external voltage, the tension imposed on the adhering vesicle increases (Fig. 3 *B*). Even though the tension increases by approximately two orders of magnitude, the absolute values of the induced tension are relatively low and orders of magnitude below the lysis tension (~10 mN/m). This result is corroborated by the membrane undulations in the unbound part of the adhering vesicles that were visible even at the highest applied external voltages. We conclude that the main energetic cost, which is balanced by the attractive potential, originates in the bending of the lipid bilayer.

We compared the data for the adhesion energy obtained from the whole-contour analysis with results obtained via a second method, namely using the contact curvature of the membrane in the contact zone with the surface (see Materials and Methods for details). The adhesion energies were calculated following both methods for 10 vesicles at different external potentials. Generally, the results from the two approaches agree well (see Fig. 4). Both methods have high uncertainties at higher adhesion energies for the following reasons: the measured parameters (e.g., area of the adhering membrane segment) used by the whole-contour method saturate toward high adhesion energies, while the contact-curvature method suffers from approaching the diffraction limit when detecting the curvature radius.

For the adhesion energies explored here, the membrane in the contact zone adopted curvatures of up to ~1/(7 μm) (see *right axis* in Fig. 4). This curvature is not very high, but the use of other types of electrodes (allowing access to higher potentials) might allow reaching even higher curvatures, making this approach useful for exploring curvature-driven processes in membranes.

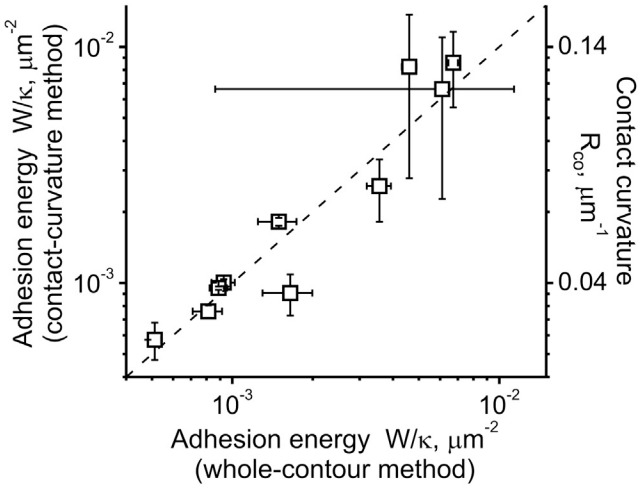

FIGURE 4 Comparison of data for the adhesion energy determined via the whole-contour method (*x* axis) and from the contact-curvature method (*left y axis*; the *right y axis* shows the membrane curvature in the contact zone, R_{co}). (*Dashed line*) Slope 1, representing ideal agreement between the two methods. The Pearson correlation coefficient is $R = 0.937$.

Redistribution of lipids in the adhering membrane segment

After having demonstrated that vesicle adhesion can be smoothly and reversibly regulated by the external potential, we investigated whether the lipid composition of the unbound and bound membrane segments is altered by the adhesion. For this purpose, we employed the fatty-acid labeled NBD-PG, which possesses the same headgroup as that of the negatively charged DOPG (see Fig. S6), and should thus reveal the behavior of this lipid as we vary the external potential. Because electrostatics might be the driving force for adhesion, the negatively charged species in the membrane may be redistributed when the external potential is applied.

During the experiments, no phase separation as characterized by micrometer-sized domains was observed under fluorescence, suggesting that the bound and unbound membrane segments remained in the same fluid phase state. The membrane fluidity was confirmed by the measured diffusion coefficient of NBD-PG determined by fluorescence recovery after photobleaching measurements. At 1.1 V external voltage, we found no difference between the diffusion coefficient measured in the adhering membrane segment and the vesicle cap, suggesting that diffusion of the bound membrane is not hindered by the adhesion process. The diffusion coefficient of NBD-PG was found to be 2.4 $\pm$ 0.2 μm^2/s.

We compared the apparently free diffusion in the bound part of the membrane in our system to diffusion in SLBs (35) prepared on ITO surfaces (i.e., the same substrate material as in our setup). The diffusion in such SLBs is slower by a factor of 1/2 compared to that in freestanding bilayers (35). We conclude that the lack of slowdown in the lipid diffusion in our system is due to weak adhesion and, thus, to a relatively thick water layer between membrane and substrate in our setup.

Even though the fluidity and diffusivity in the adhering membrane segment is not altered, measurements of the fluorescence intensity of the NBD-PG probe in the adhering membrane segment suggest that the lipid composition in this segment changes during the adhesion process. Fig. 5 shows typical results for the fluorescence intensity in the adhering membrane segment of a GUV normalized by the value in the absence of applied potential. With the onset of adhesion, the normalized fluorescent intensity drops down. This intensity change is caused by the migration of the dye from the adhering segment to the unbound vesicle cap. We exclude the possibility of a change in fluorescent brightness of NBD-PG in the adhering membrane segment because the overall fluorescence intensity of the vesicle is preserved during the voltage sweep. In addition, NBD fluorescence was found to be constant in the pH range between

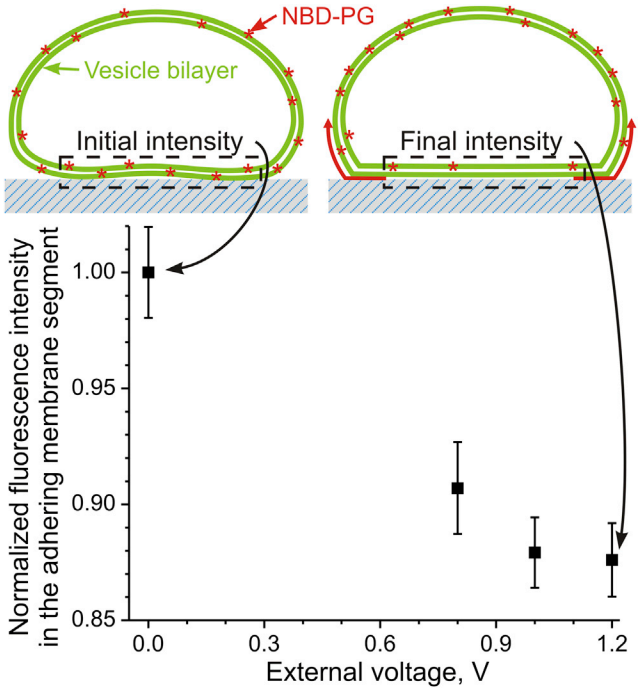

FIGURE 5 Normalized fluorescence intensity from NBD-PG in the adhering membrane segment of an unquenched vesicle exposed to different external potentials corresponding to different adhesion strengths (see Fig. 3). The sketches in the top line illustrate the depletion of NBD-PG in the adhering membrane segment (*red asterisks*) from the outer leaflet of the bound segment upon adhesion to the substrate (see text for details).

pH 5 and pH 9 (36). To exclude effects of nonradiative energy transfer from the dye to the ITO electrode (quenching), we performed control experiments using the fluorescent analog NBD-PC (see structure in Fig. S6) and found no significant quenching effect, as shown in Fig. S7. Bleaching of the dye was also not observed for the employed laser intensities and exposure times (data not shown). Because NBD-PG is depleted from the adhering membrane segment, we expect that the intensity in the cap of the vesicle would increase resulting from dye enrichment (see sketches in Fig. 5). However, the analysis and measurements in single-vesicle experiments (see Quenching Assay and Fluorescence Intensity Measurements and Fig. S2) were too imprecise because of the presence of membrane shape fluctuations with amplitudes in the micrometer range. In addition, because of the larger area of the unbound membrane compared to that of the adhering membrane segment, the expected increase in fluorescence should be smaller than the intensity change of ~10% measured for the adhering membrane segment. In other words, the expected change in brightness of several percent is below the accuracy of the measurements in the cap region.

To further examine the changes in bilayer composition in the adhering membrane segment and to probe whether the dye depletion occurs in both leaflets, we performed a quenching assay, in which the fluorescence of the outer leaflets of the vesicles before exposing them to adhesion is quenched irreversibly by sodium dithionite. We then measured the fluorescence intensity from the inner leaflet of the vesicle as a function of applied potential, similarly to the measurements in Fig. 5 on unquenched vesicles. To obtain statistically significant data, we quantified the fluorescence intensity ratio of adhering to free membrane segment of an ensemble of vesicles exposed to different external potentials and hence adhesion strengths. The raw data are shown in Fig. 6 in terms of the ratio of the fluorescent intensity of the bound to the unbound membrane segment. While for unquenched vesicles (with fluorescence from both leaflets), adhesion energies and fluorescence ratio

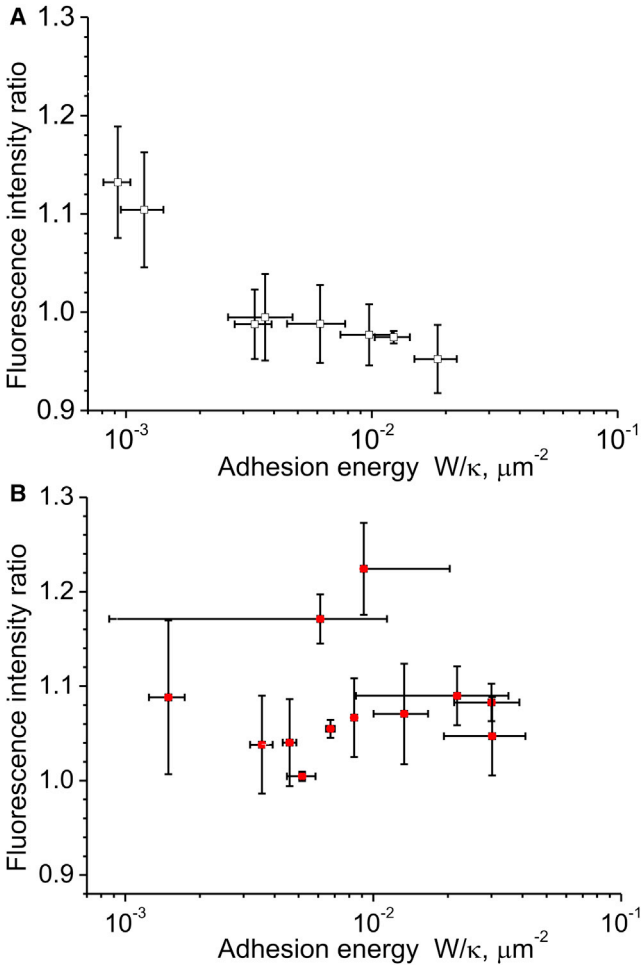

FIGURE 6 Ratio of fluorescence intensity measured in the adhering and free membrane segments for two different ensembles of vesicles: unquenched (*A*) and with quenched external leaflet (*B*). The vesicles were imaged at different external potentials and the corresponding adhesion energies were then calculated by the whole-contour method. In the unquenched vesicles, the dye is depleted from the adhering membrane segment with increasing adhesion. For the vesicles with quenched external leaflet (*B*), no such trend is observed, suggesting that the applied external potential and the adhesion process induce dye redistribution only in the external leaflet of the bilayer membrane. To see this figure in color, go online.

of adhering to unbound membrane segment were found to be highly correlated (Spearman's rank correlation coefficient $\rho < 0.0001$, $n = 8$), fluorescent intensity and adhesion energy for quenched vesicles (fluorescent signal form the inner leaflet only) was not correlated significantly ($\rho = 0.37$, $n = 12$). This outcome suggests that only the outer leaflet senses the changes in the surface potential of the ITO glasses. Asymmetric bilayers close to planar surfaces have been previously described, particularly in the context of SLB formation by liposome rupture (37–41). An important difference is the proposed mechanism of asymmetry generation by 1) lipid flip-flop between the two membrane leaflets and/or 2) pore formation. In our system, lipid flip-flop is unlikely to occur on the timescales of the observations, while pore formation is implausible in the low-tension regime explored here. Finally, no bilayer defects are observed in our system. Another important difference is the transient nature of liposome adhesion, rupture, and SLB formation compared to the stably adhering vesicles in our system. The only SLB system that is similar to our GUV system is described in Stanglmaier et al. (40), in which bilayer asymmetry is established by diffusion between the different membrane segments.

For the unquenched vesicle in Fig. 5, the change in fluorescence intensity in the adhering membrane segment amounts to a decrease of ~12% at the highest applied voltage. Assuming that the dye is depleted only in the outer membrane leaflet, leaving the inner one unaltered (as also suggested by our quenching experiments), this would imply that ~25% of the lipid dye has migrated from the adhering membrane segment to the vesicle cap.

Electrostatic interactions and lipid redistribution in the vesicle

The depletion of the negatively charged NBD-PG from the adhering membrane segment is somewhat puzzling. Initially, we expected enrichment of the negatively charged molecules in the adhering membrane segment due to the positive charge on the ITO electrode, but our data do not confirm this expectation. In this section, we show that the observed depletion of negatively charged lipids with increasing external positive potentials can be rationalized, by allowing the membrane-surface distance to vary with the external potential. To explain this effect, we first need to understand which forces act on the lipids in the two membrane segments (free and adhering).

We find no evidence for a significant electrostatic field inside the solution chamber, which could result in pulling the vesicles toward the electrode surface (via electrodeformation or electrophoresis). This conclusion is based on two observations. First, we measured the electric current between the ITO glasses and the DC voltage source. In the explored voltage range, the current always stayed <5 μA. Taking the contact area between the vesicle suspension and the ITO glass to be ~79 mm^2 and the measured conductivity of the buffer to be ~250 μS/cm, we find ~6.25 V/m for the electric field. This field strength is two orders-of-magnitude lower than the electric field typically needed for vesicle electrodeformation (42,43). Second, we filled the chamber with vesicles in pure sucrose solution (no glucose/sucrose asymmetry present across the membrane) where gravitational forces on the vesicles are absent and the vesicles are freely floating in the bulk of the chamber. Upon application of the external potential, the vesicles did not experience any drag toward the bottom electrode and no morphological changes were observed over hours. We therefore conclude that there is only insignificant charge transfer into the solution and that the external potential indeed mainly alters the electrode surface potential. The surface charge is then screened within the Debye length (~7 nm) in the vicinity of the electrodes. This is also corroborated by the measured pH value, which was found to be approximately constant over the used voltage range (see Fig. S8), indicating an insignificant amount of products from electrochemical reactions at the electrode.

We then considered short-range forces at the ITO-coated substrate. Around neutral pH, the ITO surface exhibits a negative surface charge (31). When we conducted the experiments in high salt concentrations (100 mM NaCl), for which the electrostatic interactions become screened and short-ranged, the vesicles were found not to adhere at any applied voltage. Hence, van der Waals forces alone seem not to be sufficient to establish vesicle adhesion and electrostatic forces are driving the observed adhesion.

Coulomb interactions are screened by the free ions in solution and we examine this effect using the Poisson-Boltzmann theory for ion condensation around charged bodies in solutions. We begin with some general considerations and present more detailed calculations further below. In the Debye-Hückel limit of low surface potentials and ignoring edge effects, the electrostatic pressure Π between two charged surfaces with surface charge densities σ_1 and σ_2 and positioned at a distance D is proportional to (44)

$$\Pi(D) \sim \frac{\sigma_1\sigma_2 \cosh(D/\lambda) + \sigma_1^2 + \sigma_2^2}{2 \sinh^2(D/\lambda)}. \qquad (10)$$

For large separations and oppositely charged plates, the pressure is attractive and reflecting the intuition that the attraction is proportional to charge density on either surface. In the limit of small separations, the pressure scales as $\Pi(D) \sim (\sigma_1 + \sigma_2)^2/(2 \sinh^2(D/\lambda))$ and is always repulsive, including for opposite signs of the surface charge densities, except for the special case of $\sigma_1 = -\sigma_2$. This effect can be understood by the overlap of the ion clouds as the two plates approach. Because of the requirement of electroneutrality, there is always a finite number of charges between the two plates. This builds up osmotic pressure and hence repulsion on small plate separations. The above

expression was derived for the boundary condition of fixed charges. In our system, the charges in the adhering membrane segment are not fixed but mobile. Lipid exchange can occur via lateral diffusion between the adhering and the free membrane segment (constrained by the entropic and electrostatic cost of the lipid exchange). Thus, for adhesion to be observed, the surface charge of the adhering membrane segment should readjust with changing voltage to reach an optimal density of charged lipids that is close to the charge density on the ITO surface. This will be associated with a decrease in the amount of charged ions in the membrane-surface gap.

In the absence of the applied external voltage, the surface potential of the electrode is negative. The application of the external potential shifts it toward the point of zero charge (electrically neutral). The onset of electrostatic attraction is expected to start at low positive potentials (and low surface charge density at the ITO electrode). The unperturbed lipid bilayer has a rather high surface charge of ~ -0.04 C/m^2 (assuming one elementary charge per DOPG lipid and taking 70 Å^2 for the lipid area). Hence, when adhesion is induced, the adhering membrane segment should be depleted of negative charges to match the surface charges on the ITO electrode, as observed in our experiment.

Using existing models, we attempted to assess the magnitude of charge regulation resulting from the lipid mobility. The effect of surface charge regulation resulting from lateral lipid mobility was considered in Harries et al. (29) and May et al. (30) for the case of DNA and protein absorption on lipid bilayers. We numerically solved the charge-regulated Poisson-Boltzmann equation for a planar-adhering membrane segment allowing the bilayer/surface distance to vary (see Materials and Methods). We set the voltage at which adhesion is induced, i.e., the potential of zero charge, to 0.8 V, as observed in our experiments (Fig. 3). Depending on the surface charge on the electrode (by the applied potential) and varying the bilayer/surface distance, we calculate the membrane surface charge, which can be related to the normalized fluorescence intensity as measured in the experiments (Fig. 7). Adhesion to the positively charged electrode can be observed for a wide range of potentials and membrane-surface distances. As expected from the reasoning above, the negatively charged lipids can be expelled from the adhering membrane segment (corresponding to the area below the *solid black curve*) if the membrane-to-surface distance is allowed to vary. We have indicated the measured fluorescent intensities at different voltages (data from Fig. 5). Note that we accounted for depletion of the outer bilayer only, as measured independently by the quenching experiments. The calculation suggests that the bilayer-surface separation varies between 2 and 8 nm, which is of the typical order of magnitude for membrane-surface distances found in SLBs (45). The deduced change of the membrane to surface distance is within the resolution of surface-sensitive optical interference techniques such as reflection interference contrast microscopy, making these predictions experimentally accessible. Additionally, these results imply the possibility to modulate the proximity of a lipid bilayer to an electrode by application of an external voltage with a high precision of ~15 nm/V.

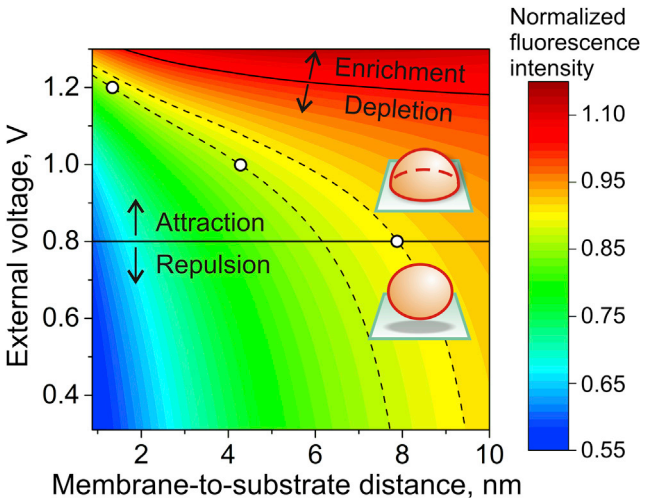

FIGURE 7 Color map of the simulated charge of the adhering membrane segment (corresponding to the normalized fluorescence intensity measured experimentally as in Fig. 5) at different bilayer-surface distances and external voltages. (*Horizontal solid line* and *cartoons*) Schematic indication of the onset of adhesion as experimentally measured. (*Open black circles*) Observed experimental fluorescent intensity data for the applied voltage (see Fig. 5).

We also tested the variation in the results accounting for errors in the used parameters. Uncertainties in the assumed Debye length correspond directly to changes in the extracted membrane-electrode distance (note that in the numerical calculations, the membrane-to-surface distance is scaled by the Debye length). Thus, we expect the extracted membrane-surface distance to be a rough estimate only. However, the conclusion about the depletion of the negatively charged dye remains valid.

The numerical calculations presented here suggest that the observed depletion of negative changes with increasing voltage requires a decrease in the membrane-substrate separation distance. This can be understood in the following way. At smaller membrane-surface distances, the osmotic pressure of the overlapping ion clouds should increase, but the system lowers its energy by slightly discharging the membrane (thus lowering the ion density in the gap and the associated osmotic pressure). It is worth noting that other membrane interactions such as undulation-, hydration-, and van der Waals-forces are not considered here and hence we do not calculate an energetic minimum. Nevertheless, it seems plausible that an increase in the external voltage (stronger adhesion) can reduce the membrane-surface distance within the calculated values.

In this way, we demonstrated that our experimental observations could be understood in terms of the electrostatic

interactions, when the screening ion clouds are described by Poisson-Boltzmann theory and the distance between the membrane and the electrode surface is allowed to vary. Finally, we considered the limit of high adhesion energies, where the membrane-surface distance must converge to a finite minimal distance. Here the calculations indicate that negative charges can accumulate with increasing positive voltage and enrichment of the charged dye should be observed (*upper-right segment* in Fig. 7), as expected for unscreened Coulomb interactions. In our experimental setup, this limit was not accessible.

CONCLUSIONS

We have developed a method to induce adhesion of GUVs to a planar substrate surface based on the application of an external potential. The adhesion strength can be smoothly regulated by turning the knob of the DC source. To calculate the adhesion energies, we used a method that relies on the overall vesicle shape as obtained via confocal microscopy. This is advantageous because adhesion energies of GUVs are usually assessed using sophisticated techniques such as reflection interference contrast microscopy and for high adhesion energies. In this study, the adhesion energies are in the weak adhesion regime because of the limited voltage range explored. This limitation is due to the onset of an electrical current by the initiation of electrochemical reaction on the substrate surface at higher potentials. Within the range of voltages applied here, we do not exceed the range of potentials for which the ITO is ideally polarizable (31). The limiting voltage is a property of the used electrode material (ITO) and, presumably, can be increased by passivation of the surface by, e.g., a polymer layer as used in electrowetting applications. Our approach for inducing controlled and tunable adhesion of vesicles to a substrate is easy to implement and, depending on the electrode polarity, it should also be applicable to positively charged membranes.

We found depletion of the negatively charged membrane species NBD-PG in the unbound segment of the vesicle. We showed that this redistribution of charged lipids is consistent with a Poisson-Boltzmann-based theoretical model, which explicitly accounts for lipid mobility. Quenching experiments have shown that only the outer leaflet composition of the bound membrane segment is changed by the interaction with the support. This suggests that (compositional) interleaflet coupling is weak in fluid DOPC/DOPG membranes. We also note that the asymmetric lipid distribution should generate nonzero spontaneous curvature in the membrane, whereas the theoretical analysis was done for zero spontaneous curvature. In general, the lipid redistribution may lead to different values of the spontaneous curvature in the bound and unbound membrane segments. Our results imply that even relatively weak nonspecific forces can induce asymmetry and thus spontaneous curvature in biomimetic and biological membranes, therefore remodeling membrane compartments (46). Finally, we have shown that diffusion in the bound membrane segment is hardly hindered compared to that in the unbound membrane. This result might be also relevant for experimental approaches employing supported membrane bilayers (as, e.g., in studies based on total internal reflection fluorescence). Compared to commonly used SLBs, in our system, there is only a minimal membrane-surface interaction and the bilayer is practically uncoupled. We also note that the vesicles become effectively immobilized on the ITO surface and do not move due to convection, which would otherwise affect quantitative fluorescence measurements. This immobilization may in practice be employed in studies of membrane properties. We also found that the electric field could be used to precisely tune the electrode-membrane distance, opening possible applications in actuating soft matter and investigating the functions of proteins incorporated in the membrane as a function of their distance to the substrate. Combined with lateral control over the distribution in the membrane and tethered vesicles (see, e.g., Yoshina-Ishii and Boxer (47)), our approach offers possibilities for a variety of membrane manipulation approaches based on the use of electric fields. Future experiments on GUVs composed of ternary lipid mixtures will provide insight into possible adhesion-induced domain formation as predicted by recent theoretical work (48).

SUPPORTING MATERIAL

Eight figures are available at http://www.biophysj.org/biophysj/supplemental/S0006-3495(16)30751-2.

AUTHOR CONTRIBUTIONS

J.S. designed and performed experiments and did the numerical calculations; R.L. designed experiments and contributed to the data analysis; R.D. designed experiments; and J.A.-C. performed the vesicle contour analysis for extracting the adhesion energy. All authors wrote and edited the article.

ACKNOWLEDGMENTS

J.S. thanks V. Georgiev for help with the fluctuation analysis and R. Knorr for the pH calibration measurements of the SNARF dye.

Financial support from the Deutsche Forschungsgemeinschaft via grant No. IRTG 1524 is gratefully acknowledged. This work is part of the MaxSynBio consortium, which is jointly funded by the Federal Ministry of Education and Research of Germany and the Max Planck Society.

REFERENCES

1. Dimova, R., S. Aranda, …, R. Lipowsky. 2006. A practical guide to giant vesicles. Probing the membrane nanoregime via optical microscopy. *J. Phys. Condens. Matter.* 18:S1151–S1176.

2. Walde, P., K. Cosentino, …, P. Stano. 2010. Giant vesicles: preparations and applications. *ChemBioChem.* 11:848–865.

3. Dimova, R. 2012. Giant vesicles: a biomimetic tool for membrane characterization. *In* Advances in Planar Lipid Bilayers and Liposomes. A. Iglič, editor. Academic Press, New York, pp. 1–50.
4. Fenz, S. F., and K. Sengupta. 2012. Giant vesicles as cell models. *Integr. Biol. (Camb).* 4:982–995.
5. Seifert, U., and R. Lipowsky. 1990. Adhesion of vesicles. *Phys. Rev. A.* 42:4768–4771.
6. Rädler, J., and E. Sackmann. 1992. Vesicle-substrate interaction studied by reflection interference contrast microscopy. *In* The Structure and Conformation of Amphiphilic Membranes. R. Lipowsky, D. Richter, and K. Kremer, editors. Springer, Berlin, Germany, pp. 158–161.
7. Fang, N., V. Chan, and K. T. Wan. 2003. The effect of electrostatics on the contact mechanics of adherent phospholipid vesicles. *Colloids Surf. B Biointerfaces.* 27:83–94.
8. Lipowsky, R., M. Brinkmann, …, X. Z. Zhang. 2005. Droplets, bubbles, and vesicles at chemically structured surfaces. *J. Phys. Condens. Matter.* 17:S537–S558.
9. Gruhn, T., T. Franke, …, R. Lipowsky. 2007. Novel method for measuring the adhesion energy of vesicles. *Langmuir.* 23:5423–5429.
10. Limozin, L., and K. Sengupta. 2009. Quantitative reflection interference contrast microscopy (RICM) in soft matter and cell adhesion. *ChemPhysChem.* 10:2752–2768.
11. Bernard, A. L., M. A. Guedeau-Boudeville, …, J. M. di Meglio. 1999. Imaging vesicle adhesion by evanescent wave-induced fluorescence. *Europhys. Lett.* 46:101–106.
12. Bernard, A. L., M. A. Guedeau-Boudeville, …, J. M. di Meglio. 2000. Strong adhesion of giant vesicles on surfaces: dynamics and permeability. *Langmuir.* 16:6809–6820.
13. Schmidt, D., C. Monzel, …, A. S. Smith. 2014. Signature of a nonharmonic potential as revealed from a consistent shape and fluctuation analysis of an adherent membrane. *Phys. Rev. X.* 4:021023.
14. Nardi, J., T. Feder, …, E. Sackmann. 1997. Electrostatic adhesion between fluid membranes: phase separation and blistering. *Europhys. Lett.* 37:371–376.
15. Nardi, J., R. Bruinsma, and E. Sackmann. 1998. Adhesion-induced reorganization of charged fluid membranes. *Phys. Rev. E Stat. Phys. Plasmas Fluids Relat. Interdiscip. Topics.* 58:6340–6354.
16. Kumar, K., C. S. Tang, …, E. Reimhult. 2009. Formation of supported lipid bilayers on indium tin oxide for dynamically-patterned membrane-functionalized microelectrode arrays. *Lab Chip.* 9:718–725.
17. Sapper, A., B. Reiss, …, J. Wegener. 2006. Adsorption and fluctuations of giant liposomes studied by electrochemical impedance measurements. *Langmuir.* 22:676–680.
18. Mugele, F., and J. C. Baret. 2005. Electrowetting: from basics to applications. *J. Phys. Condens. Matter.* 17:R705–R774.
19. Mugele, F. 2009. Fundamental challenges in electrowetting: from equilibrium shapes to contact angle saturation and drop dynamics. *Soft Matter.* 5:3377–3384.
20. Angelova, M. I., and D. S. Dimitrov. 1986. Liposome electroformation. *Faraday Discuss.* 81:303–311.
21. Bezlyepkina, N., R. S. Gracià, …, R. Dimova. 2013. Phase diagram and tie-line determination for the ternary mixture DOPC/eSM/cholesterol. *Biophys. J.* 104:1456–1464.
22. Gracià, R. S., N. Bezlyepkina, …, R. Dimova. 2010. Effect of cholesterol on the rigidity of saturated and unsaturated membranes: fluctuation and electrodeformation analysis of giant vesicles. *Soft Matter.* 6:1472–1482.
23. Cevc, G. 1993. Electrostatic characterization of liposomes. *Chem. Phys. Lipids.* 64:163–186.
24. McIntyre, J. C., and R. G. Sleight. 1991. Fluorescence assay for phospholipid membrane asymmetry. *Biochemistry.* 30:11819–11827.
25. Soumpasis, D. M. 1983. Theoretical analysis of fluorescence photobleaching recovery experiments. *Biophys. J.* 41:95–97.
26. Lipowsky, R., and U. Seifert. 1991. Adhesion of vesicles and membranes. *Mol. Cryst. Liq. Cryst.* 202:17–25.
27. Tordeux, C., J. B. Fournier, and P. Galatola. 2002. Analytical characterization of adhering vesicles. *Phys. Rev. E Stat. Nonlin. Soft Matter Phys.* 65:041912.
28. Lipowsky, R. 2014. Coupling of bending and stretching deformations in vesicle membranes. *Adv. Colloid Interface Sci.* 208:14–24.
29. Harries, D., S. May, …, A. Ben-Shaul. 1998. Structure, stability, and thermodynamics of lamellar DNA-lipid complexes. *Biophys. J.* 75:159–173.
30. May, S., D. Harries, and A. Ben-Shaul. 2000. Lipid demixing and protein-protein interactions in the adsorption of charged proteins on mixed membranes. *Biophys. J.* 79:1747–1760.
31. Hillebrandt, H., and M. Tanaka. 2001. Electrochemical characterization of self-assembled alkylsiloxane monolayers on indium-tin oxide (ITO) semiconductor electrodes. *J. Phys. Chem. B.* 105:4270–4276.
32. Vitkova, V., J. Genova, and I. Bivas. 2004. Permeability and the hidden area of lipid bilayers. *Eur. Biophys. J.* 33:706–714.
33. Mertins, O., and R. Dimova. 2013. Insights on the interactions of chitosan with phospholipid vesicles. Part II: membrane stiffening and pore formation. *Langmuir.* 29:14552–14559.
34. Dimova, R. 2014. Recent developments in the field of bending rigidity measurements on membranes. *Adv. Colloid Interface Sci.* 208: 225–234.
35. Przybylo, M., J. Sýkora, …, M. Hof. 2006. Lipid diffusion in giant unilamellar vesicles is more than 2 times faster than in supported phospholipid bilayers under identical conditions. *Langmuir.* 22:9096–9099.
36. Moreau, R. A. 1989. An evaluation of NBD-phospholipids as substrates for the measurement of phospholipase and lipase activities. *Lipids.* 24:691–699.
37. Richter, R. P., N. Maury, and A. R. Brisson. 2005. On the effect of the solid support on the interleaflet distribution of lipids in supported lipid bilayers. *Langmuir.* 21:299–304.
38. Khan, T. R., H. M. Grandin, …, I. Reviakine. 2008. Lipid redistribution in phosphatidylserine-containing vesicles adsorbing on titania. *Biointerphases.* 3:FA90–FA95.
39. Shreve, A. P., M. C. Howland, …, A. N. Parikh. 2008. Evidence for leaflet-dependent redistribution of charged molecules in fluid supported phospholipid bilayers. *Langmuir.* 24:13250–13253.
40. Stanglmaier, S., S. Hertrich, …, B. Nickel. 2012. Asymmetric distribution of anionic phospholipids in supported lipid bilayers. *Langmuir.* 28:10818–10821.
41. Wacklin, H. P. 2011. Composition and asymmetry in supported membranes formed by vesicle fusion. *Langmuir.* 27:7698–7707.
42. Aranda, S., K. A. Riske, …, R. Dimova. 2008. Morphological transitions of vesicles induced by alternating electric fields. *Biophys. J.* 95:L19–L21.
43. Salipante, P. F., R. L. Knorr, …, P. M. Vlahovska. 2012. Electrodeformation method for measuring the capacitance of bilayer membranes. *Soft Matter.* 8:3810–3816.
44. Ben-Yaakov, D., and D. Andelman. 2010. Revisiting the Poisson-Boltzmann theory: charge surfaces, multivalent ions and inter-plate forces. *Phys. A.* 389:2956–2961.
45. Kim, J., G. Kim, and P. S. Cremer. 2001. Investigations of water structure at the solid/liquid interface in the presence of supported lipid bilayers by vibrational sum frequency spectroscopy. *Langmuir.* 17: 7255–7260.
46. Lipowsky, R. 2014. Remodeling of membrane compartments: some consequences of membrane fluidity. *Biol. Chem.* 395:253–274.
47. Yoshina-Ishii, C., and S. G. Boxer. 2006. Controlling two-dimensional tethered vesicle motion using an electric field: interplay of electrophoresis and electro-osmosis. *Langmuir.* 22:2384–2391.
48. Lipowsky, R., T. Rouhiparkouhi, …, T. R. Weikl. 2013. Domain formation in cholesterol-phospholipid membranes exposed to adhesive surfaces or environments. *Soft Matter.* 9:8438–8453.

Biophysical Journal, Volume *111*

Supplemental Information

Modulating Vesicle Adhesion by Electric Fields

Jan Steinkühler, Jaime Agudo-Canalejo, Reinhard Lipowsky, and Rumiana Dimova

Supporting Information

Modulating vesicle adhesion by electric fields

J. Steinkühler, J. Agudo-Canalejo, R. Lipowsky and R. Dimova*

Max Planck Institute of Colloids and Interfaces, Science Park Golm, 14424 Potsdam, Germany

* Corresponding author: dimova@mpikg.mpg.de

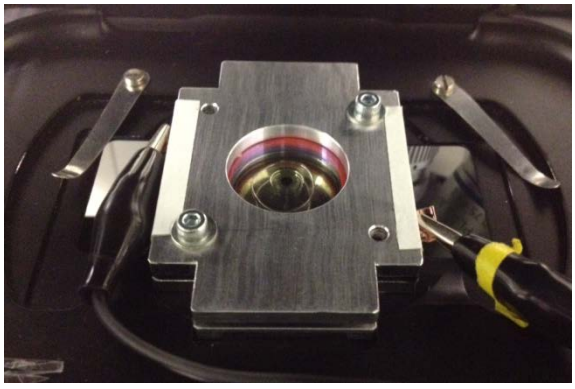

Figure S1. Picture of the experimental chamber fixed on an inverted confocal microscope. Connectors to left and right lead to the DC-voltage source. The transparent ITO glasses can be seen in the middle of the picture. The red spacer is not in contact with the vesicle suspension.

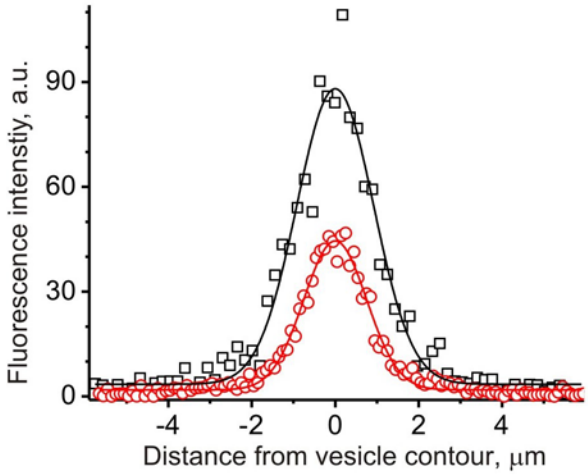

Figure S2. Examples for the intensity profiles across the membranes of an unquenched vesicle (red diamonds) and a quenched vesicle (black squares) adhering to the ITO glass. The profiles were fitted with a Gaussian (OriginPro 8.6) and the peak value taken as an indicator of dye concentration.

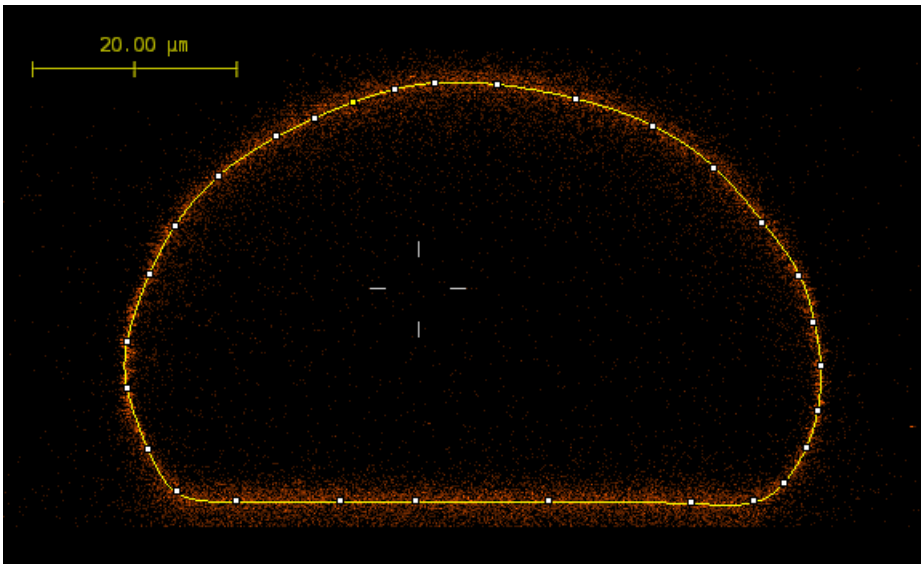

Figure S3. Image of a vertical cross section of an adhering vesicle (at 1V) as obtained by confocal microscopy. The manually determined contour (yellow) is used to compute the vesicle area and volume.

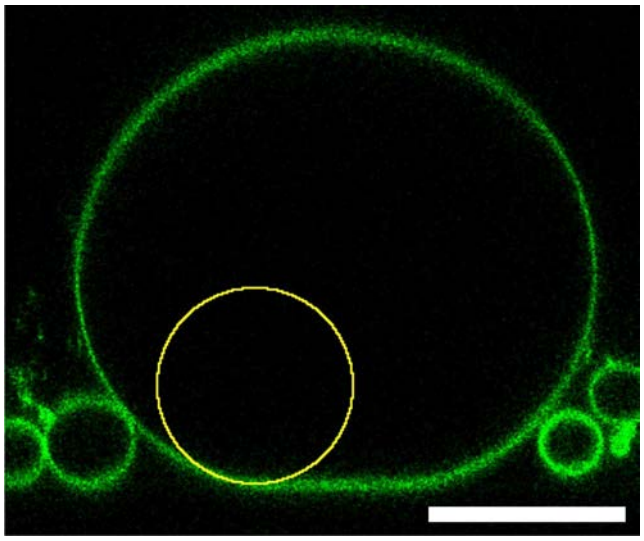

Figure S4. Measuring the contact curvature radius, R_{co}. Circle of best fit (yellow) in the contact zone of an adhering vesicle (confocal side view). The scale bar is 25µm.

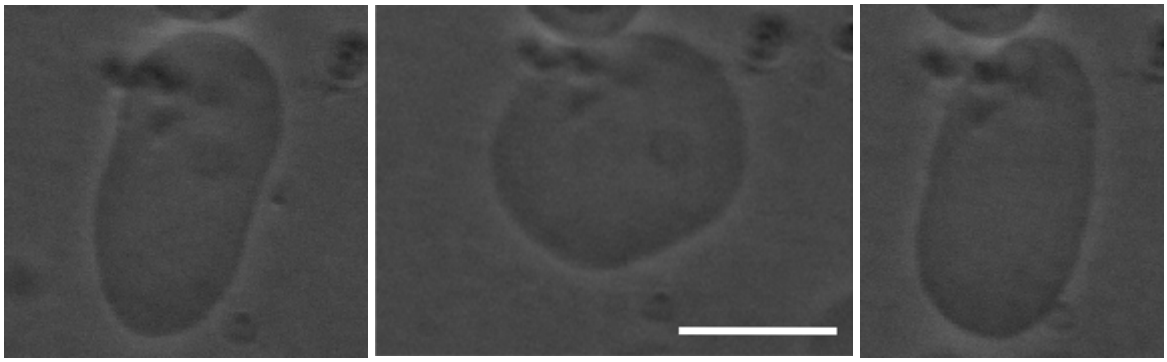

Figure S5. Phase contrast images of a very deflated vesicle consecutively exposed (from left to right) to 0V, 1.2V and 0V external voltage undergoing reversible shape changes from prolate to adhering back to prolate shape. Note the preserved contrast of the vesicle, which indicates that there is no significant leakage, consistent with the finding that the vesicle volume is preserved. Scale bar corresponds to 20µm.

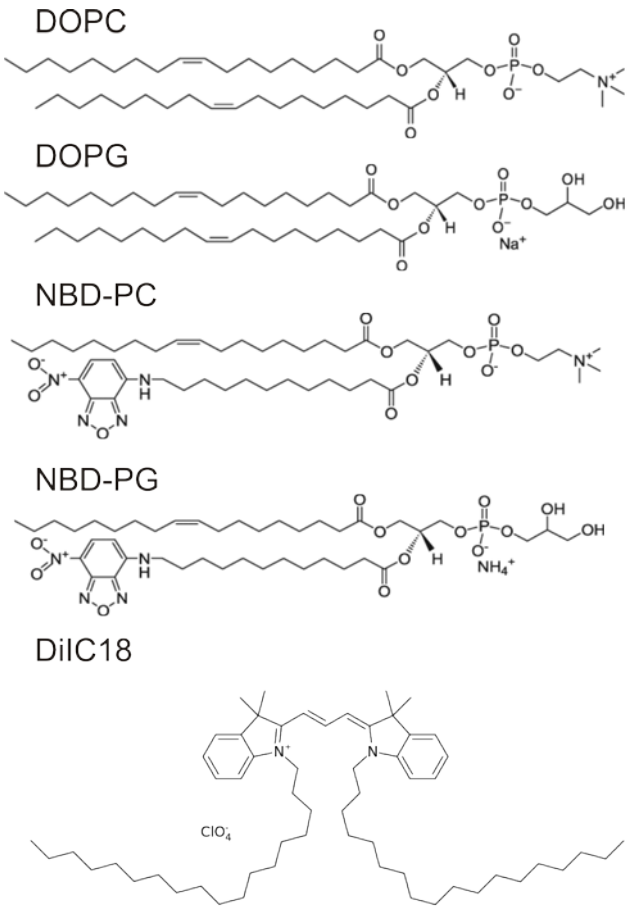

Figure S6. Structures of the lipid molecules and main fluorophores employed in this study.

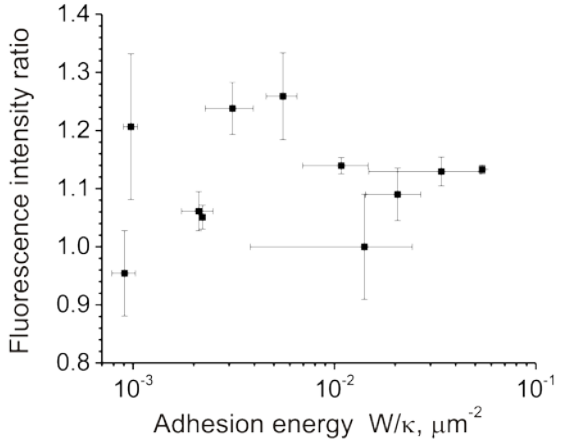

Figure S7. Fluorescent intensity ratio of adhering vesicles obtained in the same way as in Figure 6 but using a NBD labeled PC lipid analog (same label position in the acyl chain, see Fig. S6). The expected slight increase of a few percent is hidden by the uncertainty of the measurement. The absence of fluorescence quenching of NBD due to adhesion is clearly demonstrated.

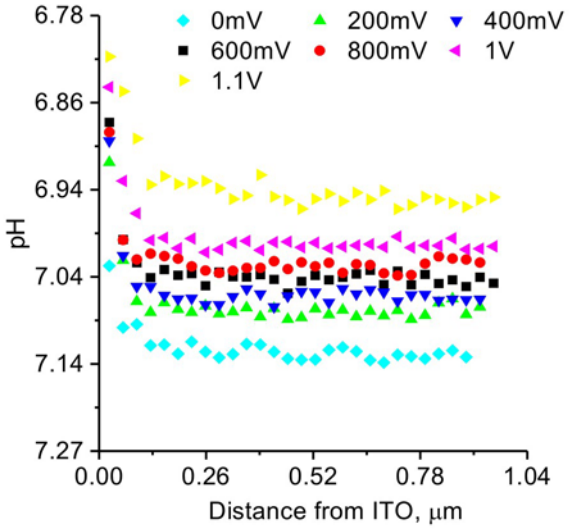

Figure S8. The pH change in the buffer near the bottom ITO glass as a function of the external potential was measured using the pH-sensitive dye SNARF (seminaphthorhodafluor, Life Technologies) which was added at concentration of 10 μM to the buffer. The intensity ratio between the green and red peak signal of the dye was converted to pH based on calibration measurements in solutions of known pH. The maximal decrease in pH was measured directly (sub μm distance) at the ITO glass surface but is still above pH 6.